0 0 0 0 4 9 0 3 6 5 3

UC-25
LBL-6993 c.1
Rev.

Lawrence Berkeley Laboratory
UNIVERSITY OF CALIFORNIA

Materials & Molecular Research Division

Submitted to the American Ceramic Society

HIGH TEMPERATURE STRESS-STRAIN BEHAVIOR OF MgO IN COMPRESSION

P. C. Dokko and J. A. Pask

January 1979

For Reference

Not to be taken from this room

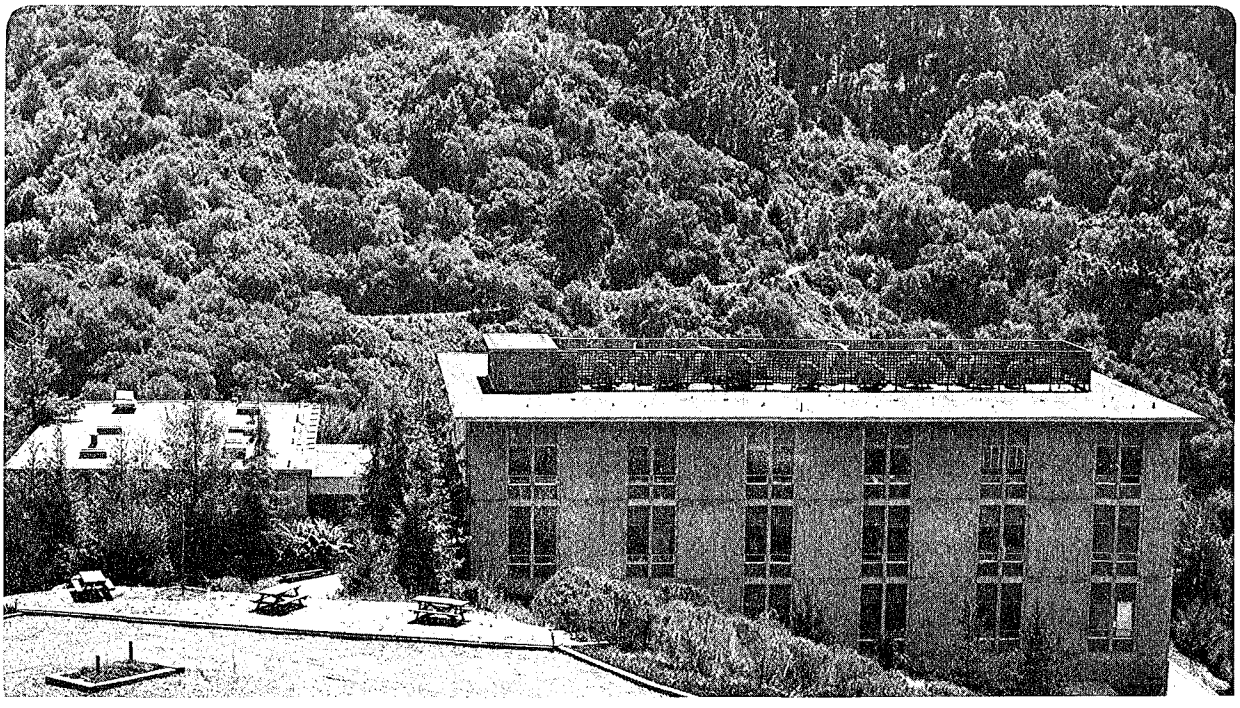

Prepared for the U. S. Department of Energy
under Contract W-7405-ENG-48

LBL-6993 c.1

LEGAL NOTICE

This report was prepared as an account of work sponsored by the United States Government. Neither the United States nor the United States Department of Energy, nor any of their employees, nor any of their contractors, subcontractors, or their employees, makes any warranty, express or implied, or assumes any legal liability or responsibility for the accuracy, completeness or usefulness of any information, apparatus, product or process disclosed, or represents that its use would not infringe privately owned rights.

U C R L 2 0 9 0 3 6 5 4

HIGH TEMPERATURE STRESS-STRAIN BEHAVIOR OF MgO IN COMPRESSION

P. C. Dokko and J. A. Pask

Materials and Molecular Research Division, Lawrence Berkeley Laboratory
and Department of Materials Science and Mineral
Engineering, University of California,
Berkeley, California

ABSTRACT

Compressive stress-strain curves for several types of polycrystalline MgO specimens were correlated with those for single crystals and analyzed as a function of grain size and grain boundary character at 1200° and 1400°C for several strain rates. The results for fully dense specimens were explained in terms of grain boundary sliding and intergranular separation in addition to slip. The modification of grain boundary nature concurrent with heat treatment for grain growth, caused by residual Li/F, was associated with enhanced grain boundary sliding and intergranular separation. For grain sizes less than 30μm, it was concluded that von Mises criteria for ductility could be relaxed by the occurrence of dislocation climb and to a limited extent by intergranular separation. Yield drop corresponding to dislocation multiplication occurred when grain boundary sliding was initially promoted. Specimens with a liquid phase of adequate viscosity also indicated plasticity accompanied by high strength. Specimens with clean grain boundaries exhibited ductility and normal strain hardening with no intergranular separation.

INTRODUCTION

When slip is the only deformation mechanism, von Mises' has pointed out that 5 independent slip systems (2 independent systems provided by easier slip on $\{110\}$ planes and 3 additional systems by more difficult slip on $\{100\}$ planes in the case of MgO) must operate for ductile deformation, i.e., without an accompanied decrease in the specimen density. While this requirement has been acknowledged as a necessary condition for ductility, it has been suggested that the condition may be relaxed by heterogeneous strain or non-slip deformation mechanisms.[2]

At high temperatures, non-slip mechanisms involving diffusion such as diffusional creep,[3,4] grain boundary sliding (GBS)[5-7] and dislocation climb[8] may become sufficiently active to play important roles. The non-slip processes may also include intergranular separation (IGS) that may temporarily dissipate stress-concentrations but eventually lead to failure.[9] These processes may occur in addition to, or in lieu of slip. Hence, the objectives of the present work are to assess the relative significance of slip and various non-slip mechanisms in high temperature deformation for polycrystalline MgO at different test conditions and deformation stages, and to study mechanical behavior under given test conditions (with emphasis on ductility) as a function of material character parameters such as grain size (GS) and grain boundary (GB) character. The susceptibility to GBS appears to be associated with such residual impurities as Li/F or glassy phase.

0 0 0 0 4 9 0 5 6 5 5

EXPERIMENTAL PROCEDURE

1. Preparation and Characterization of Specimens

Both single crystal and polycrystalline specimens of parallelepiped shape with dimensions of 3.8 x 3.8 x 7.6 mm were prepared.

Single crystal specimens, with cation impurities listed in Table I, were prepared by cleaving (for <100> orientation) or machining (for <111> orientation) the suitably oriented melt crystals* (within 1°). Machined faces were ground on a series of emery papers down to 4/0 grade. A special jig was used to ensure that the ends were parallel to each other and perpendicular to the side faces. All single crystal and polycrystalline specimens were chemically polished in 85% ortho-phosphoric acid at 110°C for 2 minutes. Also, a few single crystal specimens were annealed in air for 100 h at 1400°C prior to testing.

Three major types of polycrystalline specimens were of interest: a) Li/F- containing specimens, supplied by Eastman Kodak Co., were prepared by hot pressing with an initial 2% LiF content and then annealing to produce transparancy (probably at ~1300°C). Specimens in this (as-received) condition are designated as A0. These were annealed additionally in air for various lengths of time at 1400° and 1500°C (Type A); some specimens were annealed after being tightly wrapped in Pt foil (Type AP). All the annealed specimens remained transparent. The annealing times and corresponding grain sizes are indicated in Fig. 1 with the numbers providing specimen identification for reported mechanical tests.

---

*Muscle Shoals Electrochemical Corp., Tuscumbia, Alabama.

GS was determined as 1.27 times[10] the average chord length using the lineal intercept method, excluding occasional large grains as seen at bottom right of Fig. 12.

b) Specimens designated as Type B were fabricated by hot pressing reagent grade powder at 1275°C for 1/2 h under 25 MPa (3.6 ksi) in a graphite die. Increasing grain sizes were obtained by annealing in air at 1550°C. None of the specimens were theoretically dense (94.7% for B1, 97.5% for B3 and B4, and 97.8% for B5 specimen as determined by water immersion). The microstructures contained numerous fine intragranular pores except B1 which had primarily intergranular pores after annealing for only 2 hrs.

c) Specimens designated at Type C were obtained commercially by sintering and had a visible liquid phase at grain boundaries, particularly at triple points, as well as intragranular pores. Densities are 96.4% and 98.2% with corresponding grain sizes of 65 and 85μm for C1 and C2 specimens, respectively.

Spectrographic analysis data for these specimens are listed in Table I. Bulk contents of fluorine in several fully dense specimens annealed at 1500°C under different conditions, as determined by neutron activation analysis,[+] were AO-415, A4-390, AP3-133, and A8- less than 67 ppm. According to energy dispersive x-ray analysis, the liquid phase in C2 specimen had a composition of 63% Y_2O_3, 24% SiO_2, 5% MgO, 4% CaO and 4% Al_2O_3 by weight whereas the MgO grains had no detectable impurities. Typical micrographs of the three types of specimens are shown in Fig. 2.

[+]Dr. L. E. Kovar, General Activation Analysis, Inc., San Diego, CA.

0 0 0 0 4 9 0 3 5 5 6

2. Mechanical Testing

Specimens were subjected to compression tests in air primarily at 1200°C (0.48 Tm) and 1400°C (0.55 Tm) on an Instron testing machine. Various crosshead speeds were selected to give constant applied strain rates from 1.1×10^{-5} to 2.8×10^{-4} S^{-1}. While the majority of tests were continued until a maximum load was realized, some tests were discontinued at strains of ~10% before a maximum load was reached. Data values are given as true stress and engineering strain. True stress was chosen instead of engineering stress to indicate that a steady state was approached as achieved in some cases at later stages. Resolved shear stress was not used because of uncertainties in Taylor factor for polycrystals and for large deformations as observed in this study.

3. After-Test Examination

The surfaces of tested specimens were examined visually, optically and by scanning electron microscopy (SEM). The specimens were then mounted in resin, polished mechanically through 1/4μm diamond paste in lapping oil, and etched in a 0.5 M solution of $AlCl_3$ at 55°C for 3 minutes for optical microscopic observations.

EXPERIMENTAL RESULTS

1. Grain Growth

Average bulk GS vs. time data were obtained for type A and AP specimens at 1400 and 1500°C in air (Fig. 1). At 1500°C, grain growth (GG) followed a square law (slope of 1/2) up to a GS ~30μm, but the growth rate was considerably retarded for the AP specimens. At 1400°C, a smaller time dependence (slope of ~1/4) was followed and the growth was approximately the same for both A and AP specimens. With further heating, GG rate increased significantly (slope of 1) except for the AP specimens at 1400°C. Curved grain boundaries were observed in this range, as illustrated in Fig. 12. It is noted that GG of the wrapped specimens were faster on the surface (one or two grains deep) than in the bulk by ~2.6 times. The hot-pressed B specimens followed a cubic GG law over the entire GS range. No GG data were obtained on the sintered C specimens.

The limited F analyses indicate that residual F from the processing of specimens was being evolved during annealing and associated GG (A0 with 415 ppm in the as-received condition vs. A8 with <67 ppm after 110 h at 1500°C). The Pt wrapping retards F loss as indicated by 133 ppm after an equivalent 110 h anneal (AP3). Continuing loss of Li is also expected to occur, although the rate of loss may be different. Under these circumstances, the differences in annealing parameters between AP3 and A6 or between AP1 and A4 for the same GS undoubtedly lead to differences in GB nature, as indicated by different stress-strain behavior despite the same GS as discussed later. The absence of a wrapping effect at 1400°C must be due to low vaporization rates. The accelerated GG accompanied by development of curved grain boundaries at a GS of ~30μm may be

0 0 0 4 9 0 3 6 5 7

associated with a change in GB structure, perhaps due to a sufficient decrease in Li/F content.

2. Stress-Strain Behavior

Stress-strain curves for single crystals of <100> and <111> orientations, representing slip on primary (i.e., $\{110\}$) planes and secondary (i.e., $\{100\}$) planes, respectively, showed only continuous strain-hardening (Fig. 3). Prior annealing caused softening of the <100> crystal and hardening of the <111> crystal. Under given test conditions, all polycrystalline stress-strain curves up to fracture were bracketed by those for <100> and <111> or annealed <111> single crystals, as typified in Fig. 3 by some A specimens with GS from 4 to 162μm. With the exception of the coarsest grain A8 specimen, all A specimens tested at 1200°C and a ε of 1.1×10^{-5} S^{-1} exhibited yield drop (YD) or strain-softening of varying magnitudes. The magnitude of YD (difference between upper and lower yield points) was maximized for an intermediate GS of ~18 μm (A5). While YD was generally followed by steady state or strain-hardening stages, some YD was followed by continuous strain-softening, thus indicating a premature failure as observed in the AP1 specimen (Fig. 8) or at 1100°C (Fig. 4). The YD diminishes with increase of temperature as illustrated for A4 specimen (Fig. 4), except for A5 which retained a reduced YD at 1400°C. While YD may also be absent upon reloading after prior deformation at the same temperature, it was observed to reappear upon reloading at a lower temperature. Slight YD also occurred in C specimens whereas only continuous strain-hardening was exhibited by the B specimens except B1 which showed a small YD followed by continuous strain-softening.

The yield stress (YS) is defined as 0.1% offset stress. The GS dependences of YS at a $\dot{\varepsilon}$ of 1.1×10^{-5} S^{-1} are shown in Figs. 5 and 6 for 1200 and 1400°C, respectively. For A specimens with a small GS (<10μm at 1200°C or <30μm at 1400°C) and C specimens, YS increased with increasing GS. For A, AP and B specimens with a large GS (>30μm), on the other hand, YS decreased with increasing GS. The A and AP specimens are characterized by an unusual Hall-Petch behavior with a negative intercept whereas the B specimens follow a typical Hall-Petch relationship[11] intersecting the single crystal (<100> in this case) value. These variations in GS dependence among A and AP, B and C specimens for GS >30μm are indicative of GB effects. While the GS dependences for A and AP specimens remain essentially the same at both temperatures, the GS-dependence for the finer grain A specimens is reversed by an increase in $\dot{\varepsilon}$ by 25 times (Fig. 6). In all cases, however, the YS values are between those for <100> and <111> single crystals.

As shown in Fig. 7, the strain rate sensitivity (SRS) of YS is different between A6 and AP3 specimens (1/8 and 1/3.3, respectively) for the same GS of 28μm. This observation provides evidence for differences in GB nature as determined by different annealing methods. This figure also indicates that A0 with the smallest GS and the highest total Li/F content has the highest SRS of 1/2. The GB difference is further implied in a comparison of stress-strain curves for A6 and AP3 specimens and for A4 and AP1 specimens with an equivalent GS of 14μm (Fig. 8). As compared with the unwrapped specimens, the wrapped specimens are characterized either by higher flow stresses or by a premature failure. This figure also shows curves for the B1 and B3 specimens. The curves for

0 0 0 3 4 9 0 5 5 8

B2, B4 and B5 are similar to B3 in conformity with the microstructure feature that the pores are uniformly distributed and essentially intragranular whereas the pores in B1 are intergranular. While it is tempting to attribute the large difference in stress-strain curves between B1 and the rest of B series to such a physical difference, it is also possible to postulate that the grain boundaries were chemically affected during hot pressing in graphite and remained so only after a short, subsequent anneal (B1). The similarity among the rest of B specimens, on the other hand, may reflect a different, constant GB structure.

A comparison of stress-strain curves at 1200° and 1400°C for 3 types of coarse-grain specimens (A7, B5 and C2) is shown in Fig. 9. The significant difference is consistent with the GB effects mentioned above for YS. The greatest temperature effect on the nature of stress-strain curves exhibited by the glass- containing C specimen suggests that the behavior depends strongly on the relative viscosities of the glass at the two temperatures. The curves also provide information on relative fracture stresses and strains.

The fracture stress (FS) is defined as a maximum or a steady state stress reached after YD. Thus, FS for AP series was generally higher than UYP (except AP1 where a premature failure occurred), whereas that for A series was lower (except A7 where FS > UYP). As a result, the fracture stresses at 1200°C for AP specimens are equal to or greater than for A specimens of equivalent GS as shown in Fig. 10 (AP1 not shown). This figure also indicates that a Hall-Petch relationship with zero intercept is obeyed for FS of A and AP specimens with GS > 30μm. The FS of A specimens with GS < 30μm are essentially constant regardless of GS,

and similar to that of a <100> crystal. Similar observations are made at 1400°C.

Ductility is defined at the same point as for FS, except for the premature failure where the ductility was given at the upper yield point. These data for A and AP specimens at 1200° and 1400°C under a $\dot{\varepsilon}$ of 1.1×10^{-5} S^{-1} are plotted against $(GS)^{-1/2}$ in Fig. 11. Ductility generally decreased with increasing GS although the relationship tended to diminish for large GS. The deviations for smaller GS may reflect the variations of, and the sensitivity to the GB character after slight anneal. The GS and GB effects, however, diminish at the highest ε of 2.8×10^{-4} S^{-1} where only negligible ductilities are obtained. All B specimens show significantly large ductilities exceeding 10% as compared with ~4% for A and AP specimens on the basis of the same GS (>30μm). The C specimens are also more ductile than the A and AP counterparts at 1200°C, although the situation is reversed at 1400°C.

3. Examination of Tested Specimens

The loss of transparency, corresponding to IGS throughout the whole specimen, occurred in all A and AP specimens at early stages of deformation. At 1200°C and a ε of 1.1×10^{-5} S^{-1}, an A3 specimen (~11μm) became translucent as soon as the elastic limit was exceeded (i.e., at a plastic strain of ~0.1% which was short of its upper yield point) and became opaque at ~1.5%. However, the more ductile AO specimen showed a greater resistance to IGS as indicated by the retained transparenty up to 1.5%. IGS was observed along single grain facets approximately parallel to the compression axis. These separations increased in their width before fracture, thus suggesting their stability as microcracks.

0 0 3 0 4 9 0 3 5 5 9

In conjunction with IGS, occurrence of GBS was suggested by intrusion/extrusion of surface grains in the finer grain specimens or by fold formation in the coarser grain specimens (Fig. 12). Slip was also operative as indicated by subboundary formation for medium grain A and AP specimens (Fig. 13) and by fold formation for coarse grain A and AP specimens (Fig. 12). As also seen in Fig. 13, development of diamond-shaped grains was noted. Neither GBS nor IGS was evident in B specimens where deformation by wavy slip took place throughout the grains (Fig. 14), except B1 which showed evidence of IGS.

DISCUSSION

Deformation of MgO near 0.5 Tm takes place by GBS and possibly a diffusional mechanism in addition to slip, with their relative contributions being determined by GB character as well as GS, temperature, strain rate and deformation stages. GB cohesion is a critical factor for ductile deformation in all cases although diffusion via dislocation climb and IGS to a limited extent can also contribute to deformation. In this study, grain growth in theoretically dense A and AP series with residual Li/F was accompanied by a change in GB chemistry and/or structure. The Li/F content (either total or on the basis of GB area) changed with GS. Even if the impurity content may remain constant, GB structure may still change with time at 1500° or 1400°C, since the prior annealing temperature was ~1300°C. As a result, GS effect may be modified by the concurrent change in GB character. Specimen B1 also indicated a change in GB character in comparison with the other B specimens.

1. Slip

Slip is indicated by optical observations as mentioned previously. Furthermore, GBS and diffusional mechanisms are ruled out as a dominant mechanism when YS or FS either remains constant or decreases with increasing GS. Thus slip predominates in most cases with the exception of A or AP specimens with a small GS (<10μm at 1200°C or <30μm at 1400°C) at early stages and C specimens tested at a low strain rate.

The magnitudes of FS for A specimens with GS <30μm, similar to that of a <100> crystal, however, suggest that contribution of $\{100\}$ slip is minimized at later stages. Their considerable ductilities also suggest that GB cohesion is not generally too weak or residual additives have

0 0 - 0 4 9 0 3 6 0

other beneficial effects as well. The observed ductilities can be partly attributed to IGS that may act as an accomodation mechanism for slip, since IGS is equivalent to localized removal of GB barriers and hence to relaxation of the von Mises requirement. IGS for GS greater than 30μm, however, acts as a detrimental crack as suggested by a Hall-Petch type of behavior for FS.

The large observed ductilities with slip primarily on $\{110\}$ planes may also be attributed to the capability of dislocation climb to become an effective deformation mechanism in combination with $\{110\}$ slip as proposed by Groves and Kelly.[12] While the observed SRS (~1/5)[13] and GS insensitivity of FS is consistent with Weertman's climb and glide model,[8] the actual strain rate is somewhat lower than the calculated value (Table II). Furthermore, Weertman's model does not take the von Mises considerations into account. In association with the largest ductility, the amount of Li/F per unit GB area is actually lowest for AO specimen because of the largest GB area[19] although its total content is highest. Alternatively, it may not be unreasonable to expect enhanced diffusion in fine-grained A specimens due to the large total Li/F contents in addition to increased conbributions of GB diffusion. Under these conditions, dislocation climb may be enhanced and operation of the Groves-Kelly mechanism may be more likely. Consequently, $\{110\}$ slip accompanied by climb and/or IGS is suggested to be responsible for the large ductilities of A specimens with GS <30μm at a low strain rate. A reasonably strong GB cohesion, however, is still a requirement to ductile deformation as shown by the scatter for the slightly annealed specimens indicative of GB sensitivity (notably AP1 and B1 specimens).

2. Grain Boundary Sliding

The visual evidence of GBS throughout A and AP series indicates that GBS takes place in addition to or in lieu of slip. Since GBS is not apparent in B specimens, the presence of residual Li/F appears to promote GBS. Thus, the unusual Hall-Petch behavior of YS for the former specimens with GS >30μm may reflect the modification of intrinsic GS effect by the concurrent change in GB nature, i.e., decreasing Li/F content with increasing GS. It may be significant that an association exists between such a behavior and the accelerated grain growth mentioned earlier. On the other hand, B series (except B1 specimen which has weak GB due to intergranular pores and possibly residual carbonaceous impurities) presumably has a constant GB structure throughout GS range, thus providing a typical Hall-Petch behavior intersecting the single crystal value. In these specimens, GBS is suppressed and $\{100\}$ slip is activated at low applied stresses because of high GB stress concentrations caused by $\{110\}$ slip. The higher YS for A and AP specimens may be attributed to dissipation of the local stress concentrations by IGS. IGS occurs at very early stages in conjunction with GBS even when $\{100\}$ slip and hence all five slip systems are activated as suggested by the YS similar to that of a <111> crystal. Although ductility is ultimately limited by IGS, IGS provides some accomodation for GBS as well as slip as indicated by the widening of IGS: this widening also makes a direct contribution to an overall deformation prior to fracture as visualized by Evans.[20]

The GB effect is also shown by the different behaviors between A6 and AP3 specimens with a comparable GS, where the wrapped specimen was

0 0 0 0 4 9 0 3 6 1

annealed for a longer period thus presumably developing a different GB structure or chemistry. In comparison with the former specimen, the latter is characterized by a higher SRS and a smaller ductility at 1400°C and a higher fracture stress at both test temperatures, pointing to a greater susceptiblity to GBS.

GBS seems to be a dominant deformation mechanism in fine-grained A specimens (<10μm at 1200°C) at early stages and in C specimens under a low strain rate, both exhibiting a positive GS- dependence for YS. A high SRS (~1/2) and GS- exponent (~2) of YS accompanied by a large ductility for the AO specimen, in particular, seems to suggest that superplastic GBS[7] takes place in lieu of slip despite the YS comparable to that of a <100> crystal. Such SRS or GS- dependence of AO specimen is not maintained at a high strain rate nor at later stages under a low strain rate. In the latter, the Groves-Kelly mechanism becomes operative. Nevertheless, the continuing occurrence of GBS enhanced by Li/F is not necessarily detrimental to ductility if suitable GS and GB cohesion are obtained. Nor is GBS enhanced by glassy phase at GB detrimental as observed in a C specimen if the phase at triple points is of adequate viscosity and can deform as a grain to accomodate GBS. This behavior is indicated by the absence of strain hardening while a high strength is maintained corresponding to simultaneous deformation of MgO grains.

Yield drop is most pronounced for an intermediate GS, i.e., when yielding occurs at the same stress as a <111> crystal. In the case of A specimens, subsequent deformation occurs at the same stress as a <100> crystal, i.e., by $\{110\}$ slip (accompanied by climb and/or IGS as

discussed earlier). Hence YD must correspond to replacement of {100} slip via multiplication of {110} dislocations when {100} slip is activated throughout properly oriented grains. This interpretation is also consistent with the reappearance of YD upon reloading at a lower temperature where the increased plastic anisotropy would force more extensive {100} slip. The YD observed in this study therefore is somewhat different from the YD due to dislocation multiplication as described in the literature.[21] It is of interest to note that there appears to be an association between YD and development of diamond-shaped grains. Such a morphology has been observed earlier in crept HCP metals.[22]

3. Diffusion Contribution

Diffusional creep has been reported to occur in pure and doped MgO.[23,24] In the present study, diffusion contribution is increased with decreasing GS, particularly in fully dense specimens where total Li/F content also increases, so that diffusional creep becomes likely, accompanied by the softening effect. This may be the case at least at yielding stages (under low stress) in an AO specimen tested at a low strain rate since the predicted value based on a diffusional model (e.g. Coble's creep) is comparable to the actual value (Table II). However, the observed SRS (~1/2) and GS- exponent ($\lesssim$2)[13] is in better agreement with superplastic GBS[7] rather than diffusional creep with a linear strain rate dependence. At later stages, diffusion contributions persist as indicated by strain rate dependence and GS- dependence of ductility. The GS- insensitivity of steady flow stresses, however, suggests that superplastic GBS or diffusional creep is no longer predominant. Instead, the diffusion contribution comes in the form of

0 0 0 4 9 0 3 5 5 2

dislocation climb combined with {110} slip as discussed earlier.

CONCLUSION

1. In order to realize possible ductility slip does not need to take place on all five slip systems, if a transition to {110} slip accompanied by climb and/or IGS, shown as YD, occurs via multiplication of {110} dislocations when {100} slip is activated throughout the grains. Ductility is enhanced with a small GS and adequate GB cohesion.

2. Such residual impurities as Li/F may affect GB nature and enhance GBS while reducing GB cohesion. As a result, traditional GS effect may be modified (exaggerated in this study) by concurrent changes in GB character with a decrease in ductility. On the other hand, such impurities may also enhance lattice diffusivity and hence a susceptibility to deformation by {110} slip and climb, counteracting the other detrimental effects on ductility for GS < 30μm at low strain rates.

3. For GS > 30μm, a larger ductility accompanied by a higher fracture stress may be realized if GBS is enhanced but accommodated by a glassy phase at triple points with adequate viscosity to deform as a grain, or if the GB is sufficiently clean so that GBS and IGS are suppressed altogether.

ACKNOWLEDGMENT

This work was supported by the Division of Materials Sciences, Office of Basic Energy Sciences, U.S. Department of Energy under contract No. W-7405-Eng-48.

REFERENCES

1. R. von Mises, "Mechanik der Plastischen Formanderung von Kristallen," Z. Angew, Math. Mech. 8, 161-185 (1928).

2. M. S. Paterson, "The Ductility of Rocks" in Physics of Strength and Plasticity, ed. by A. S. Argon, pp. 377-392. MIT Press (1969).

3a. F. R. N. Nabarro, "Deformation of Crystals by the Motion of Single Ions," in Report of a Conference on Strength of Solids, pp. 75-90, The Physical Society, London (1948).

3b. C. Herring, "Diffusional Viscosity of a Polycrystalline Solid," J. Appl. Phys. 21, 437-445 (1950).

4. R. L. Coble, "A Model for Boundary Diffusion Controlled Creep of Polycrystalline Materials," J. Appl. Phys. 34, 1679-1682 (1963).

5. M. F. Ashby and R. A. Varrall, "Diffusion Accomodated Flow and Superplasticity," Acta Met. 21, 149-163 (1973).

6. T. G. Langdon, "Grain Boundary Sliding as a Deformation Mechanism during Creep," Phil. Mag. 22, 689-700 (1970).

7. R. C. Gifkins, "Grain Boundary Sliding and its Accommodation during Creep and Superplasticity," Met. Trans. 7A, 1225-1232 (1976).

8. J. Weertman, "Steady State Creep through Dislocation Climb," J. Appl. Phys. 28, 362-364 (1957).

9. A. G. Evans, C. Roy and P. L. Pratt, "The Role of Grain Boundaries in the Plastic Deformation of Calcium Fluoride," Proc. Brit. Ceram. Soc., 6, 173-188 (1966).

10. R. E. Fryxell and B. A. Chandler, "Creep, Strength, Expansion and Elastic Moduli of Sintered BeO as a Function of Grain Size, Porosity, and Grain Orientation," J. Am. Ceram. Soc., 47, 283-291 (1964).

0 0 0 0 4 9 0 5 6 6 5

11a. E. O. Hall, "The Deformation and Aging of Mild Steel. III. Discussion of Results," Proc. Phys. Soc., London, B64, 747-753 (1951).

11b. N. J. Petch, "The Cleavage Strength of Polycrystals," J. Iron Steel Inst. 174, 25-28 (1953).

12. G. W. Groves and A. Kelly, "Change of Shape Due to Dislocation Climb," Phil. Mag. 19, 977-986 (1969).

13. P. C. Dokko and J. A. Pask, unpublished.

14. J. Weertman, "Dislocation Climb Theory of Steady State Creep," Trans. Am. Soc. Met. 61, 681-694 (1968).

15. Y. Oishi and W. D. Kingery, "Oxygen Diffusion in Periclase Crystals," J. Chem. Phys. 33, 905-906 (1960).

16. D. R. McKenzie, A. W. Searcy, J. B. Holt and R. H. Condit, "Oxygen Grain Boundary Diffusion in MgO," J. Am. Ceram. Soc., 54, 188-190 (1971).

17. D. H. Chung and W. G. Lawrence, "Relation of Single-Crystal Elastic Constants to Polycrystalline Isotropic Elastic Moduli of MgO. II. Temperature Dependence," J. Am. Ceram. Soc. 47, 448-455 (1964).

18. J. Weertman, "Creep of Indium, Lead and Some of Their Alloys with Various Metals," Trans. Am. Inst. Min. Engrs. 218, 207-218 (1960).

19. P. C. Dokko, "High Temperature Deformation of MgO," Ph.D. Thesis, University of California, Berkeley. Tech. Report LBL-3979, Nov. 1975.

20. P. E. Evans, "Creep in Yttria- and Scandia-Stabilized Zirconia," J. Am. Ceram. Soc. 53, 365-369 (1970).

21. W. G. Johnston, "Yield Points and Delay Times in Single Crystals," J. Appl. Phys. 33, 2716-2730 (1962).

22. Vakil Singh, P. Rama Rao, G. J. Cocks and D. M. R. Taplin, "On the Formation of the Diamond Grain Configuration during High Temperature Creep and Fatigue," J. Mat. Sci. 12, 373-383 (1977).

23. E. M. Passmore, R. H. Duff and T. Vasilos, "Creep of Dense, Polycrystalline MgO," J. Am. Ceram. Soc. 49, 594-600 (1966).

24. G. R. Terwilliger, H. K. Bowen and R. S. Gordon, "Creep of Polycrystalline MgO and MgO-Fe_2O_3 Solid Solutions at High Temperatures," J. Am. Ceram. Soc. 53, 241-251 (1970).

Table I. Spectrographic Analysis of MgO Types.

Constituent*	Single Crystal	AO	B1	C1	C2
Mg		Principal constituent in each type			
Li		less than 0.1% in each, not detected			
B	N.D.+	N.D.+	< 0.005 %	< 0.005 %	< 0.005 %
Al	0.004 %	0.002 %	.001	.035	.01
Si	.01	.002	.015	1.0	.6
Ca	.1	.003	.02	.25	.12
Cr	.001	< .001	< .001	.001	< .001
Fe	.01	.007	N.D.	N.D.	N.D.
Ni	.001	.001	.002	.005	.004
Y	< .005	< .005	< .005	< .005	.1

*Constituents reported as oxides of the elements indicated. Analysis performed by American Spectrographic Laboratories, Inc., San Francisco, California.

+N.D. = Not Determined.

Table II. Comparison between True Observed and Calculated Strain Rates for AO Specimen (S^{-1}).

	1200°C	1400°C	
$\dot{\varepsilon}$ observed	~3.0×10^{-6}* at 107 MPa*	~8.6×10^{-6}* at 38 MPa	
	~1.5×10^{-5}+ at 169 MPa+	~1.7×10^{-5}+ at 107 MPa+	
$\dot{\varepsilon}$ calculated (Ashby-Verrall)[5]	7.0×10^{-5} 2.5×10^{-5}	1.3×10^{-5} 1.5×10^{-5}	$\frac{100\Omega}{d^2kT}\left(D + 3.3\frac{D_b\omega}{d}\right)\left(\sigma - 0.72\frac{\gamma_6}{d}\right)$
$\dot{\varepsilon}$ calculated (Coble)[4]	1.0×10^{-5} 3.6×10^{-6}	1.7×10^{-6} 1.9×10^{-6}	$\frac{47.7\Omega\ D_6\omega\sigma}{d^3kT}$
$\dot{\varepsilon}$ calculated (Nabarro-Herring)[3]	7.5×10^{-9} 4.3×10^{-9}	8.5×10^{-9} 1.3×10^{-8}	$\frac{13.3\Omega D\sigma}{d^2kT}$
$\dot{\varepsilon}$ calculated (Nabarro)[14]	3.1×10^{-7}	9.9×10^{-7}	$\frac{0.1\pi bD\sigma^3}{G^2kT}$
$\dot{\varepsilon}$ calculated (Weertman)[8]	7.6×10^{-5}	1.0×10^{-4}	$\frac{10.5D\sigma^2}{G^2b^2}\ \sin h\ \frac{0.22b^{1.5}\ \sigma 2.5}{G^{1.5}\ M^{0.5}\ kT}$

*yielding stage (0.2% strain), + steady state

where Ω = atomic volume ~$0.7b^3$ with b = Burger's vector = 2.98×10^{-10} m.

d = grain size, σ = applied stress, γ_b = grain boundary energy ~ 1 J/m^2.

D = lattice self-diffusion coefficient = $2.5 \times 10^{-10}\ e^{-261,000/RT}, m^2/s$ (15)

D_b = grain-boundary self-diffusion coefficient, ω = grain boundary width.

$D_b\omega = 6.6 \times 10^{-15}\ D^{1/2}$, m^3/s (16).

G = shear modulus = 9.8×10^4 and 9.2×10^4 MPa (17) at 1200° and 1400°C, respectively.

M = number of Frank-Read sources per unit volume = $.277\ \rho^{1.5}$ (18) with ρ = dislocation density ~10^{12} dislocations/m^2.

0 0 0 0 4 9 0 3 6 6 5

FIGURE CAPTIONS

1. Average grain size vs. time for A, AP and B type specimens.
2. Microstructure of undeformed, coarse-grained specimens a) A7, b) B4, c) C2.
3. Stress-strain curves for A type and single crystal specimens at 1200°C ($\dot{\varepsilon} = 1.1 \times 10^{-5} s^{-1}$).
4. Effects of temperature on stress-strain curves for A4 specimens at $\dot{\varepsilon} = 1.1 \times 10^{-5} s^{-1}$.
5. Yield stress vs. $(\text{grain size})^{-1/2}$ data for A, AP, B and C specimens at 1200°C ($\dot{\varepsilon} = 1.1 \times 10^{-5} s^{-1}$).
6. Yield stress vs. $(\text{grain size})^{-1/2}$ data for A, AP, B and C specimens at 1400°C ($\dot{\varepsilon} = 1.1 \times 10^{-5}$ and $2.8 \times 10^{-4} s^{-1}$).
7. Strain-rate effects on yield stress for some A and AP type and single crystal specimens at 1400°C.
8. Stress-strain curves for medium-grain A, AP and B specimens at 1200°C ($\dot{\varepsilon} = 1.1 \times 10^{-5} s^{-1}$).
9. Stress-strain curves for coarse-grain A, B and C specimens at 1200° and 1400°C ($\dot{\varepsilon} = 1.1 \times 10^{-5} s^{-1}$).
10. Fracture stress vs. $(\text{grain size})^{-1/2}$ data for A and AP specimens at 1200°C ($\dot{\varepsilon} = 1.1 \times 10^{-5} s^{-1}$).
11. Fracture strain or ductility vs. $(\text{grain size})^{-1/2}$ plot for A and AP specimens at 1200°C ($\dot{\varepsilon} = 1.1 \times 10^{-5} s^{-1}$) and 1400°C ($\dot{\varepsilon} = 1.1 \times 10^{-5}$ and $2.8 \times 10^{-4} s^{-1}$).
12. Surface of AP4 specimen deformed 5% ($\varepsilon_f \sim 4.6\%$), at 1200°C and $\dot{\varepsilon} = 1.1 \times 10^{-5} s^{-1}$: intergranular separations spread from A to C (compression axis vertical).

13. Polished section of AP3 specimens deformed 17% (ε_f ~13%) at 1400°C and $\dot{\varepsilon} = 1.1 \times 10^{-5} s^{-1}$ (compression axis vertical).

14. Surface of B5 specimen deformed 11% ($<\varepsilon_f$) at 1200°C and $\dot{\varepsilon} = 1.1 \times 10^{-5} s^{-1}$ (compression axis vertical).

0 0 0 0 4 9 0 3 6 6 6

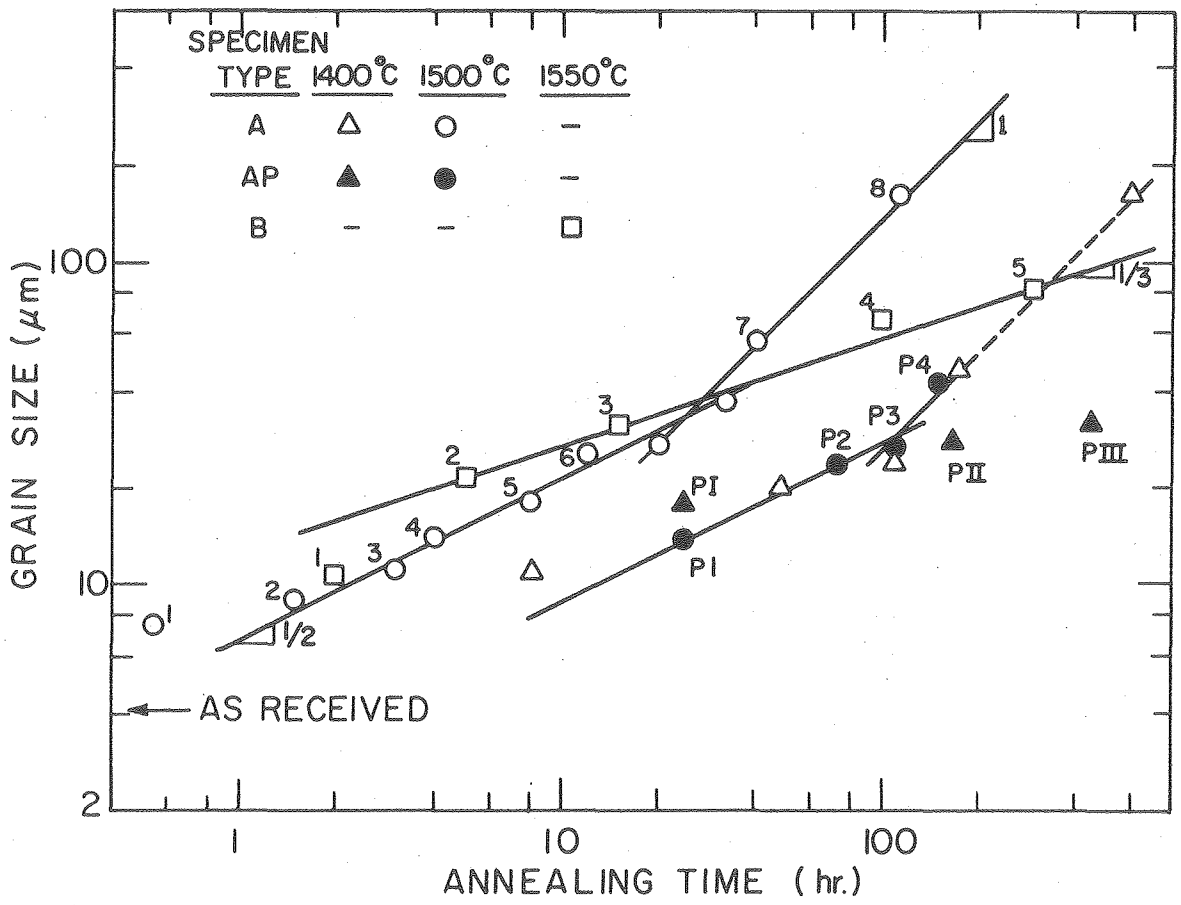

Fig. 1

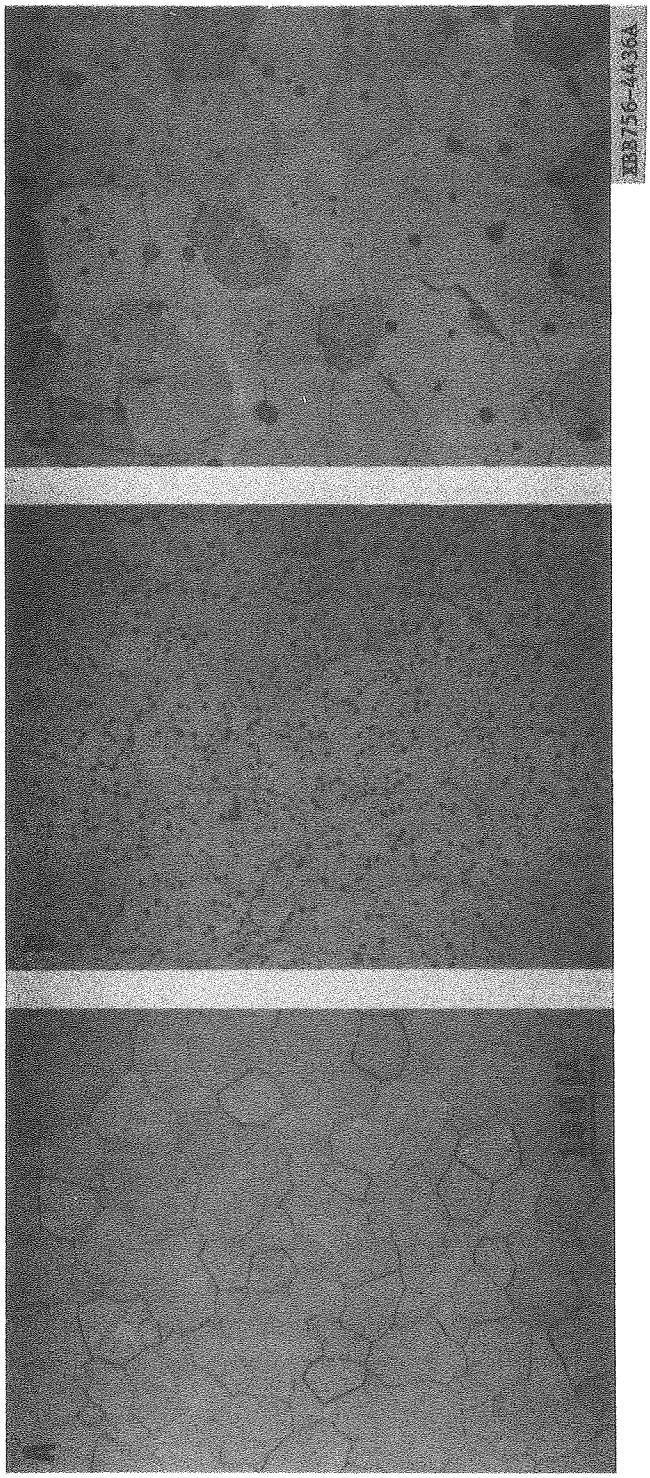

Fig. 2

0 0 0 0 4 9 9 3 6 6 7

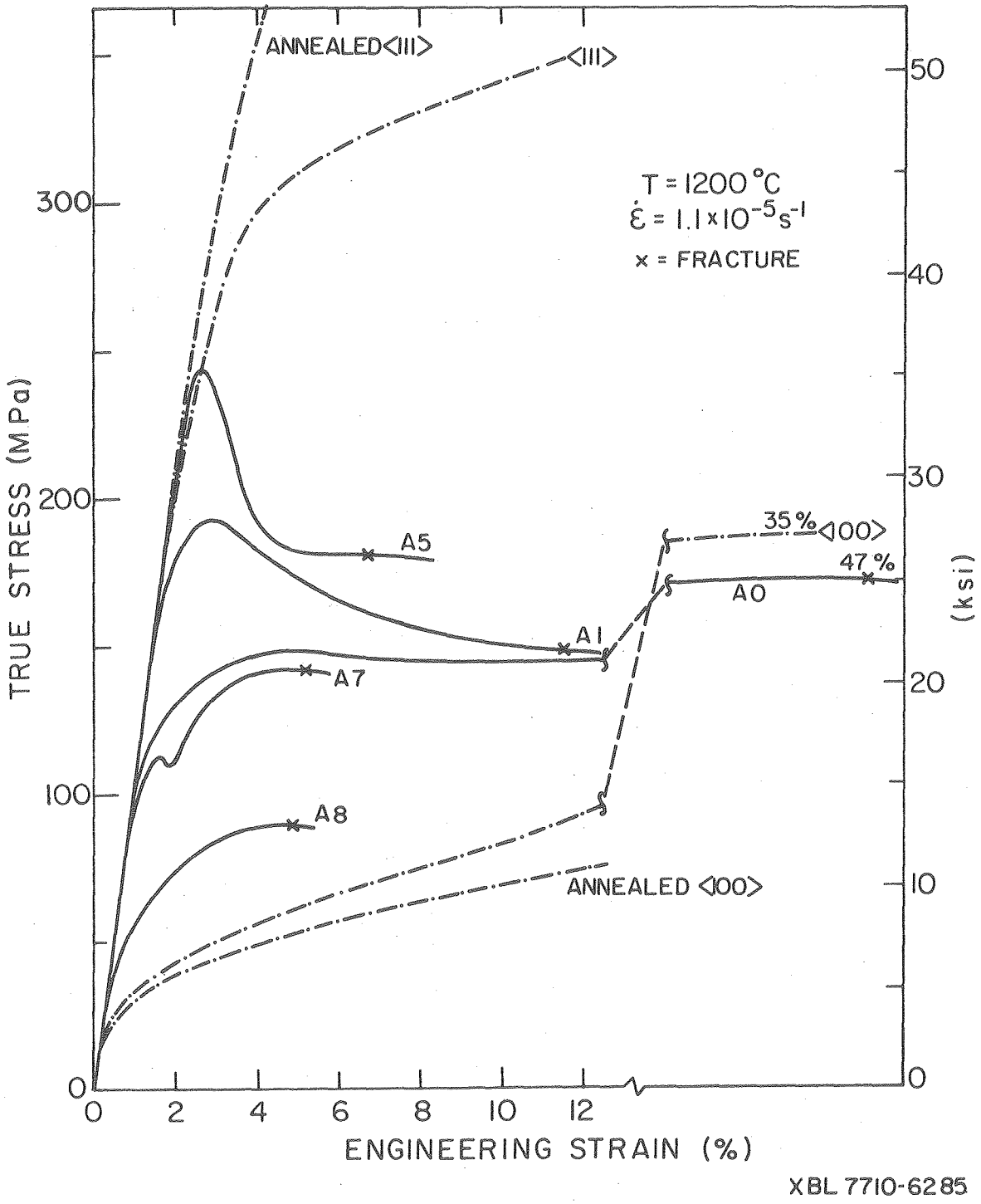

Fig. 3

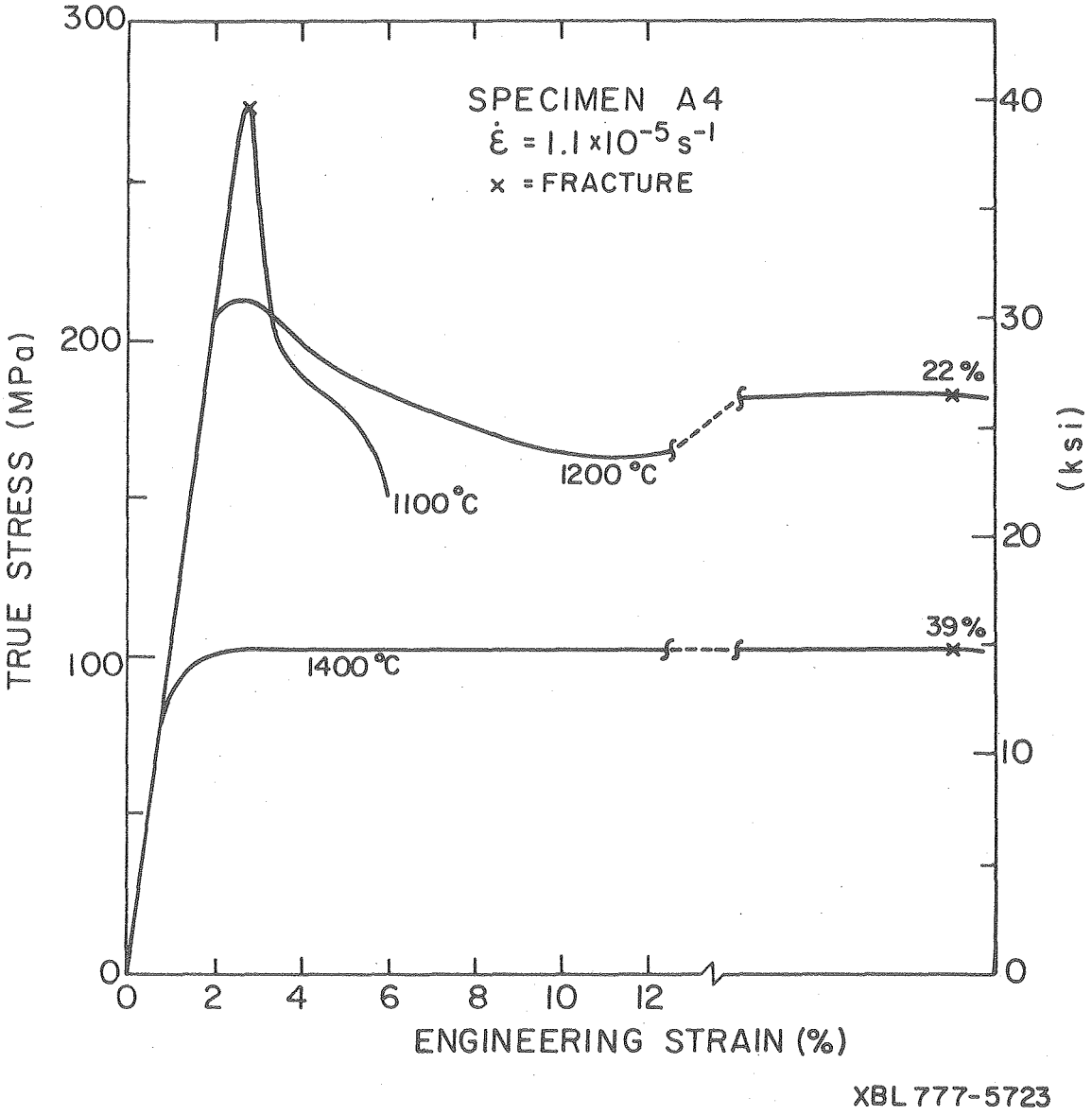
SPECIMEN A4
$\dot{\varepsilon} = 1.1 \times 10^{-5}\ s^{-1}$
x = FRACTURE
1100°C
1200°C
1400°C
22%
39%
TRUE STRESS (MPa)
(ksi)
ENGINEERING STRAIN (%)
0
100
200
300
10
20
30
40
2
4
6
8
10
12
XBL 777-5723

Fig. 4

0 0 0 0 4 9 0 5 6 8

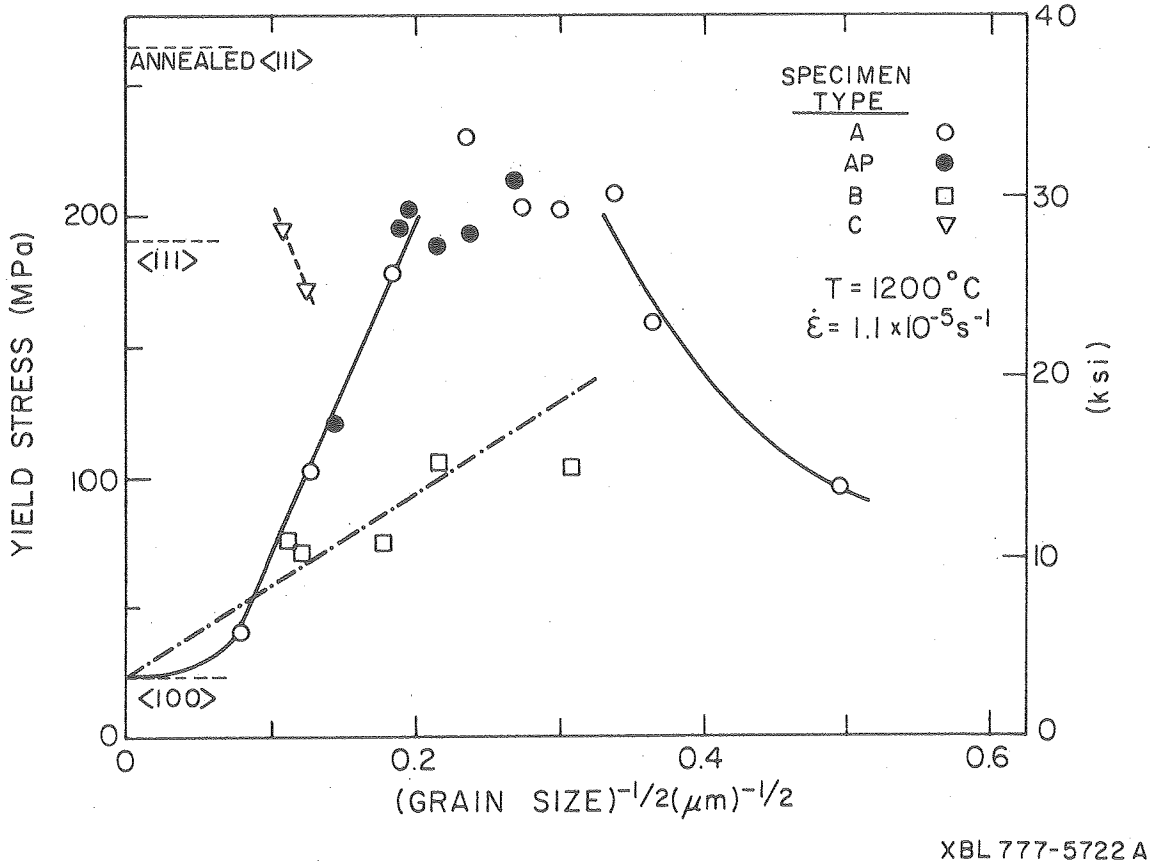

XBL 777-5722 A

Fig. 5

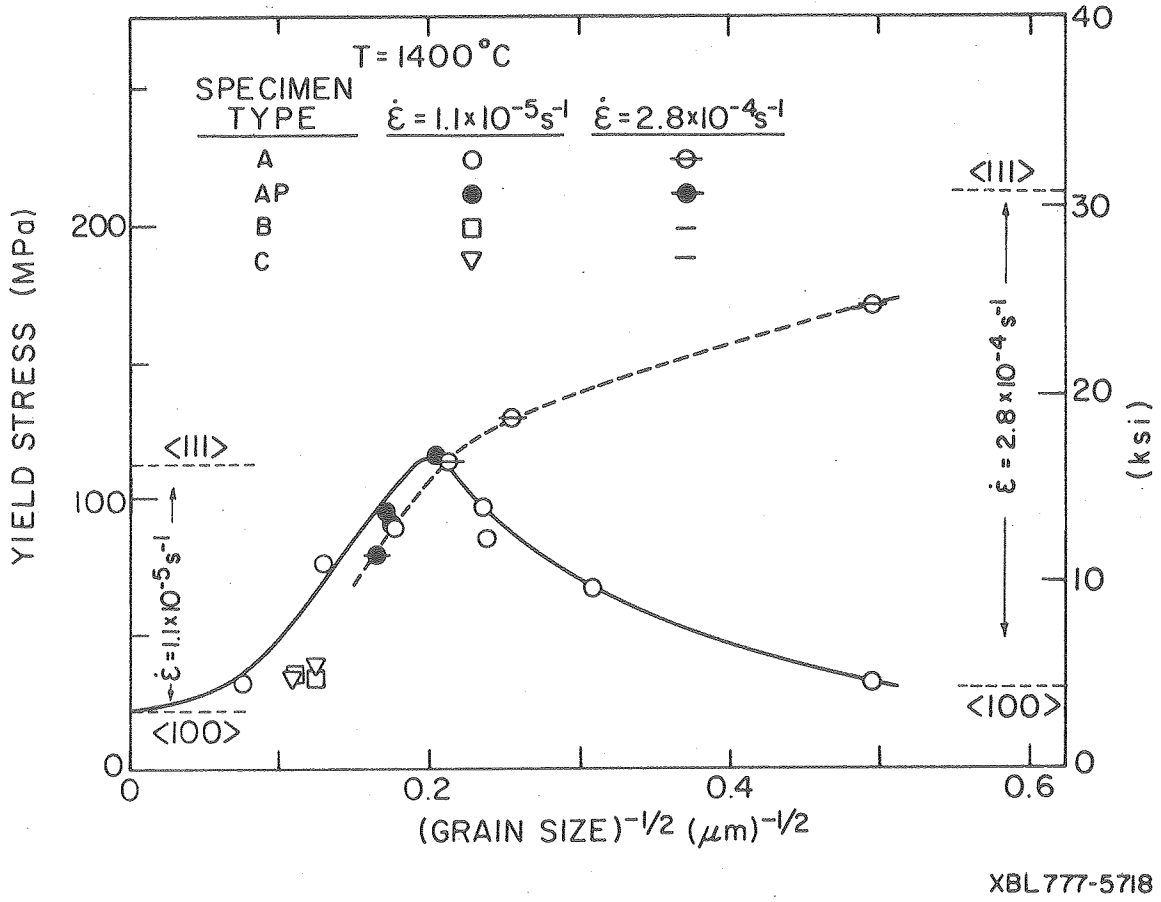
T = 1400°C
SPECIMEN TYPE
$\dot{\varepsilon} = 1.1 \times 10^{-5} s^{-1}$
$\dot{\varepsilon} = 2.8 \times 10^{-4} s^{-1}$
A
AP
B
C
YIELD STRESS (MPa)
(ksi)
<111>
<100>
$\dot{\varepsilon} = 1.1 \times 10^{-5} s^{-1}$
$\dot{\varepsilon} = 2.8 \times 10^{-4} s^{-1}$
0
100
200
10
20
30
40
0.2
0.4
0.6
(GRAIN SIZE)$^{-1/2}$ (μm)$^{-1/2}$
XBL777-5718

Fig. 6

0 0 0 0 4 9 0 3 6 6 9

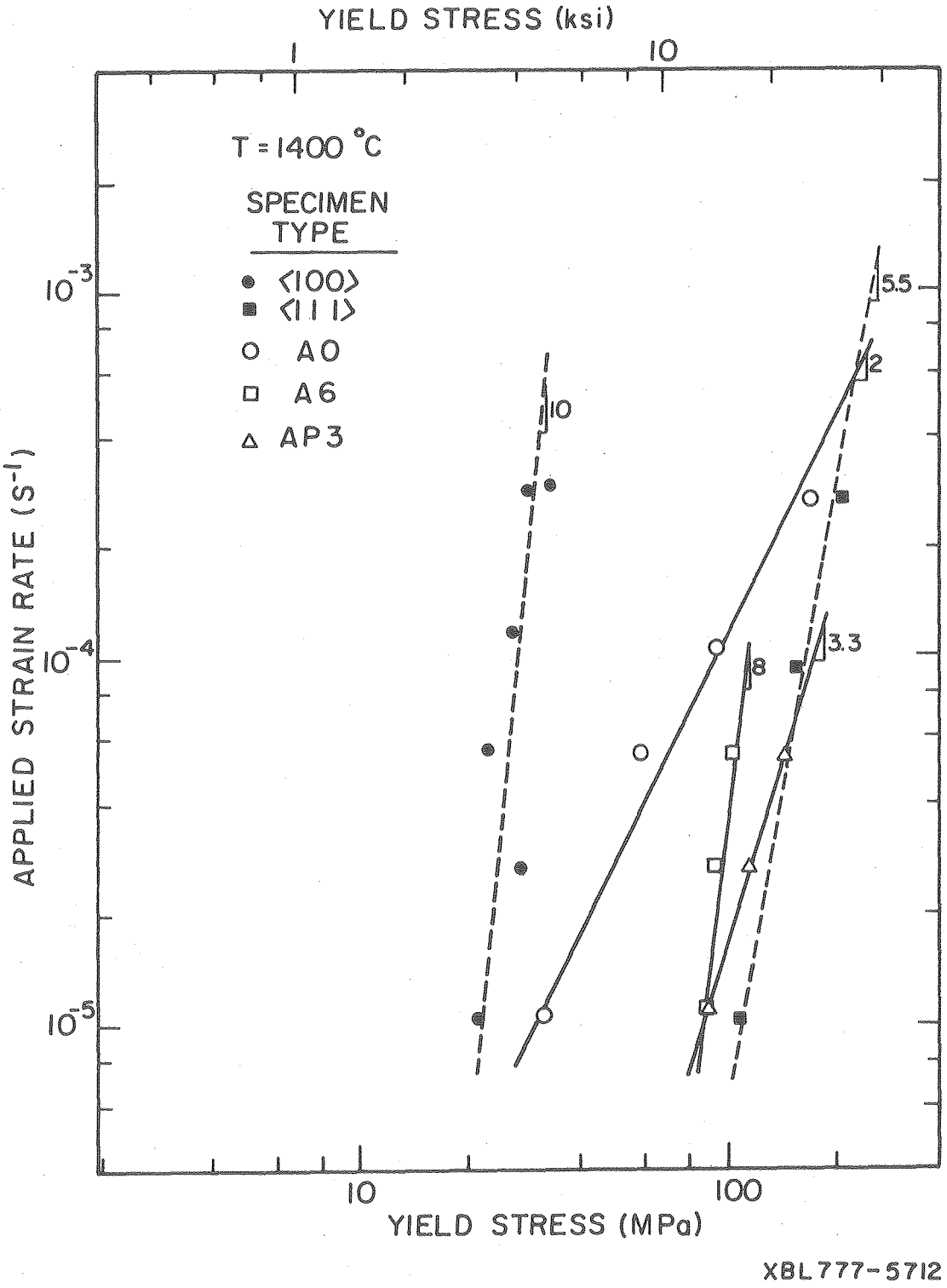

Fig. 7

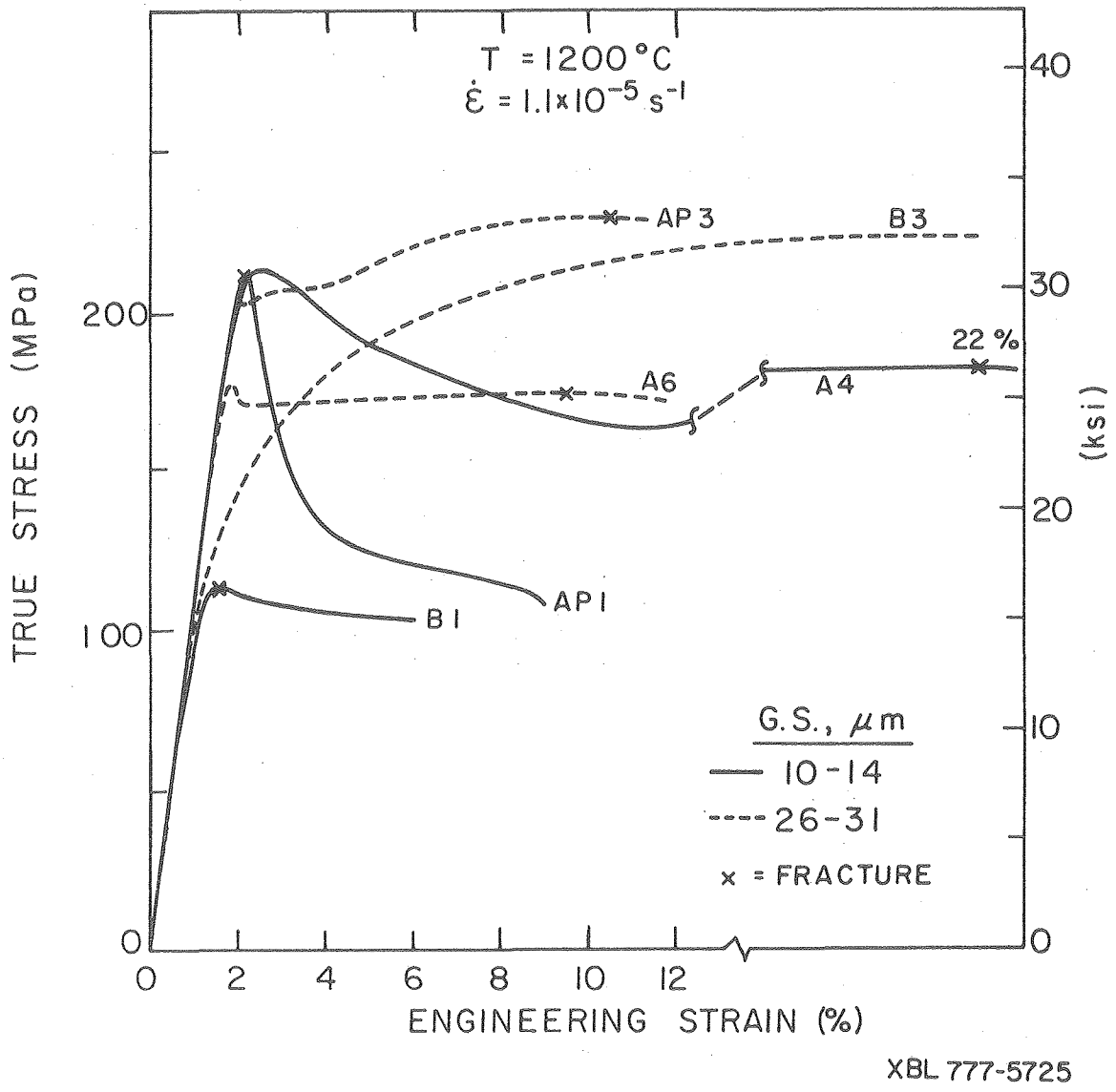
T = 1200 °C
$\dot{\varepsilon}$ = 1.1×10^{-5} s^{-1}
AP 3
B3
A6
A4
22 %
AP 1
B 1
G.S., μm
10-14
26-31
x = FRACTURE
TRUE STRESS (MPa)
(ksi)
ENGINEERING STRAIN (%)
0
100
200
0
10
20
30
40
0
2
4
6
8
10
12
XBL 777-5725

Fig. 8

0 0 0 0 4 9 0 3 6 7 0

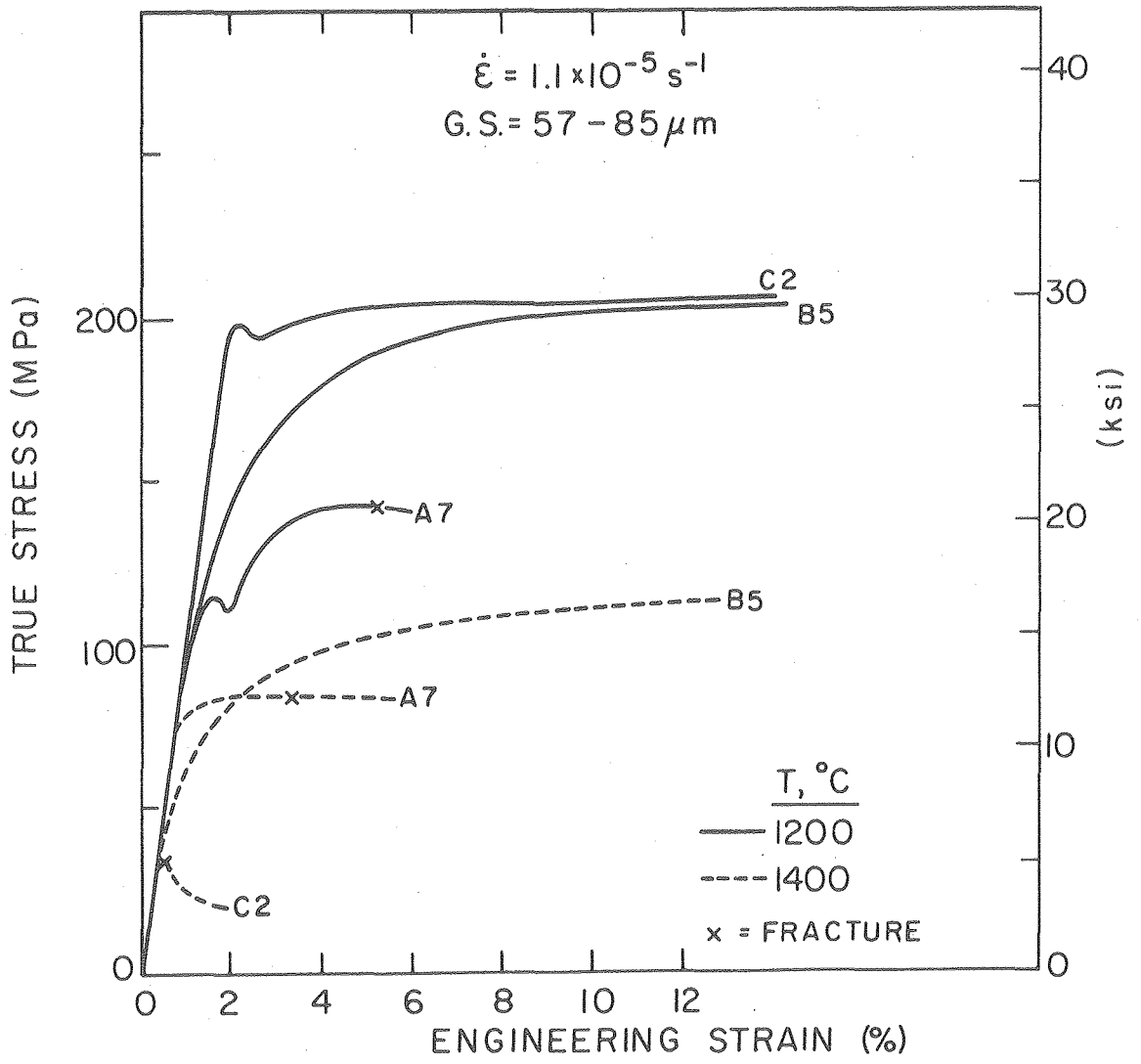

XBL 777-5726A

Fig. 9

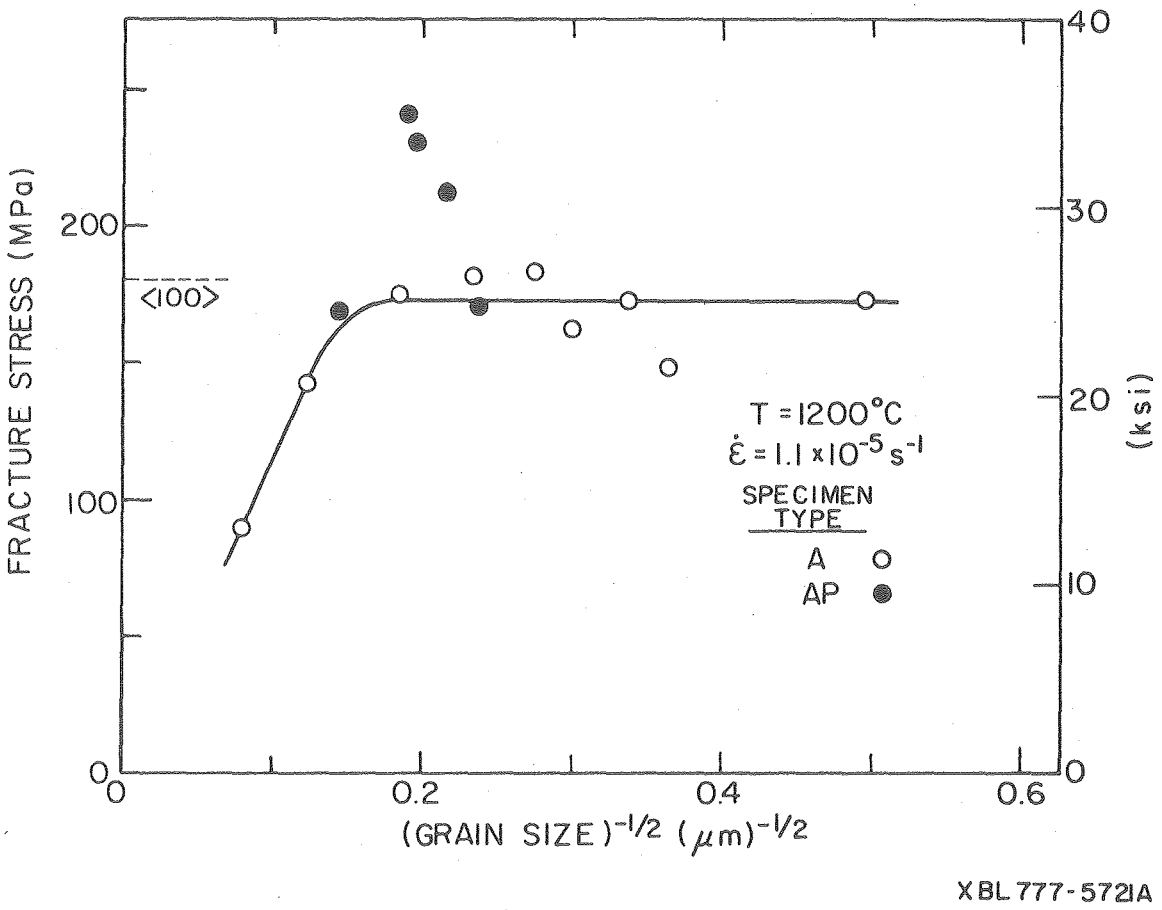
FRACTURE STRESS (MPa)
200
100
0
<100>
0
0.2
0.4
0.6
(GRAIN SIZE)$^{-1/2}$ (μm)$^{-1/2}$
40
30
20
10
0
(ksi)
T = 1200°C
$\dot{\varepsilon}$ = 1.1 x 10^{-5} s^{-1}
SPECIMEN TYPE
A
AP
XBL 777-5721A

Fig. 10

0 0 0 0 4 9 0 3 6 7 1

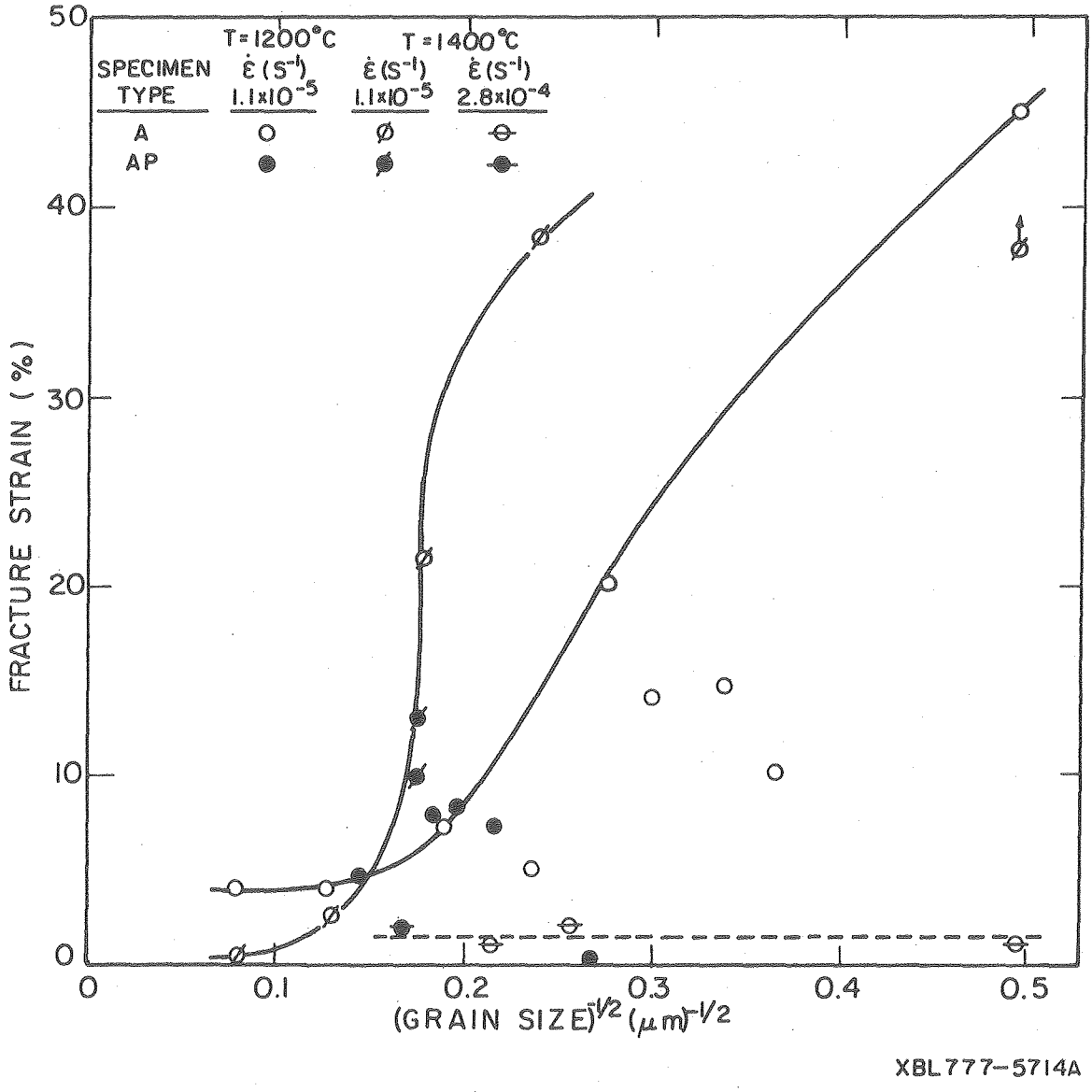

Fig. 11

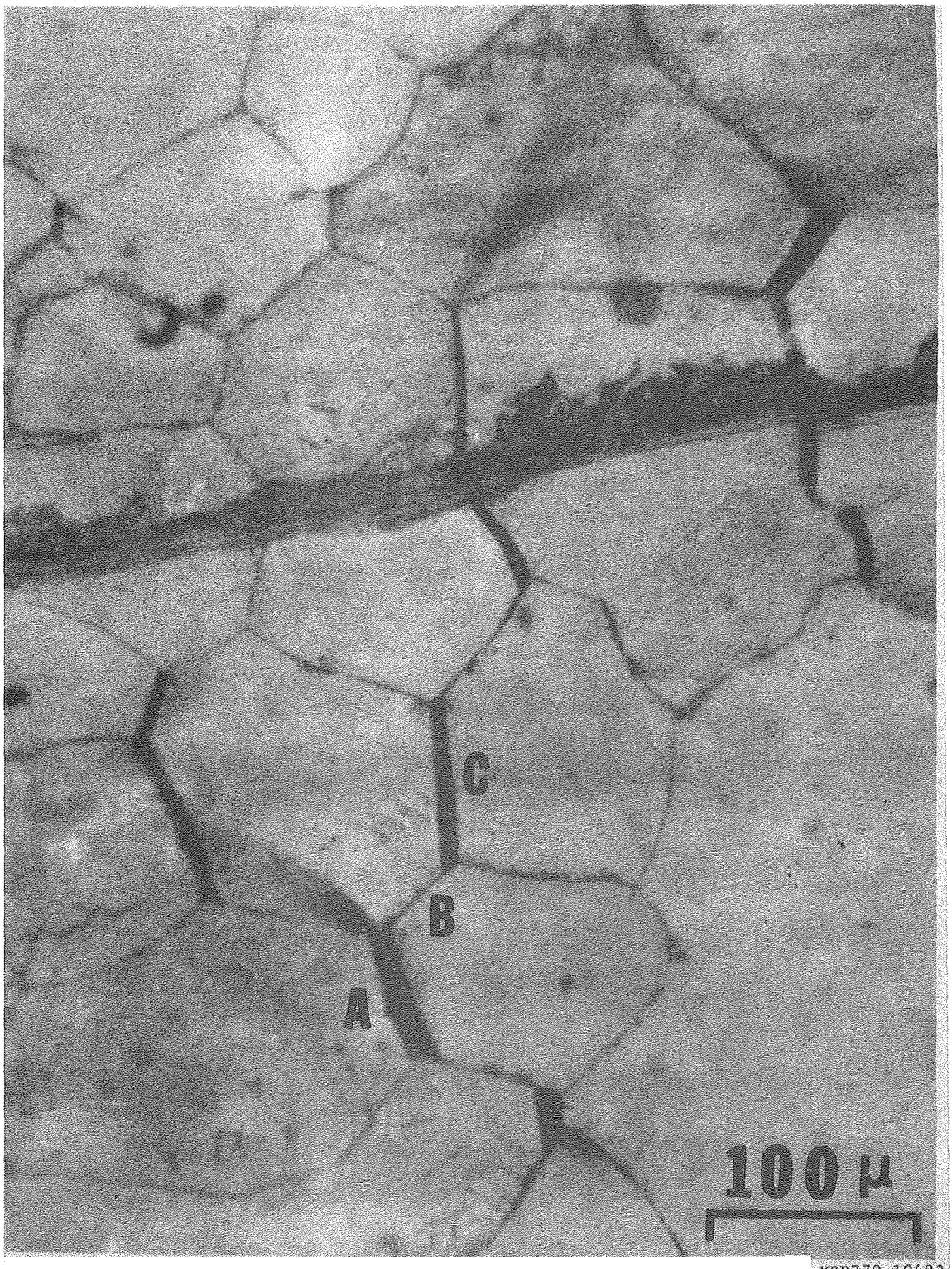
C
B
A
100 μ
XBB770-10423

0 0 0 0 4 9 0 3 6 7 2

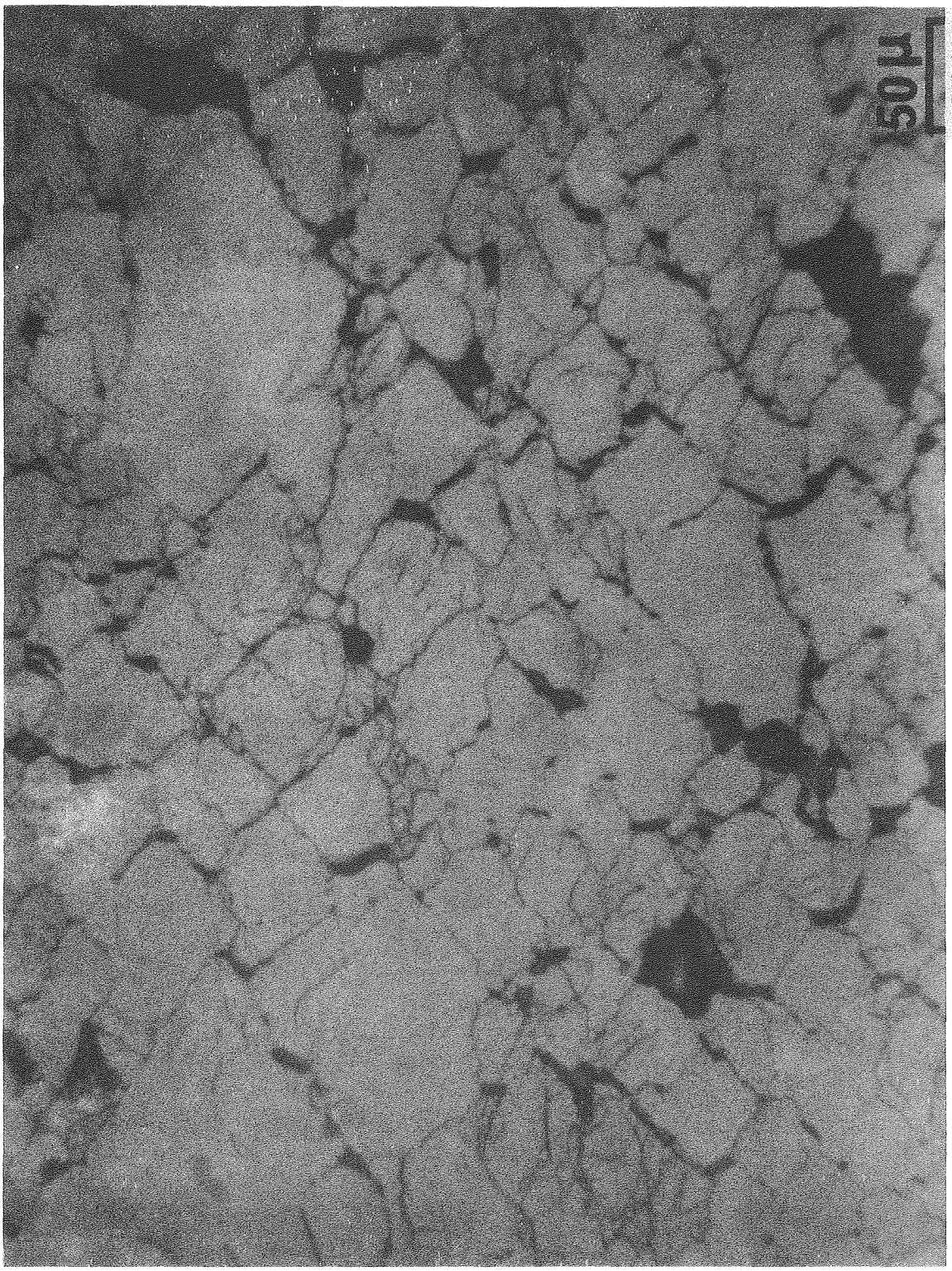

Fig. 13

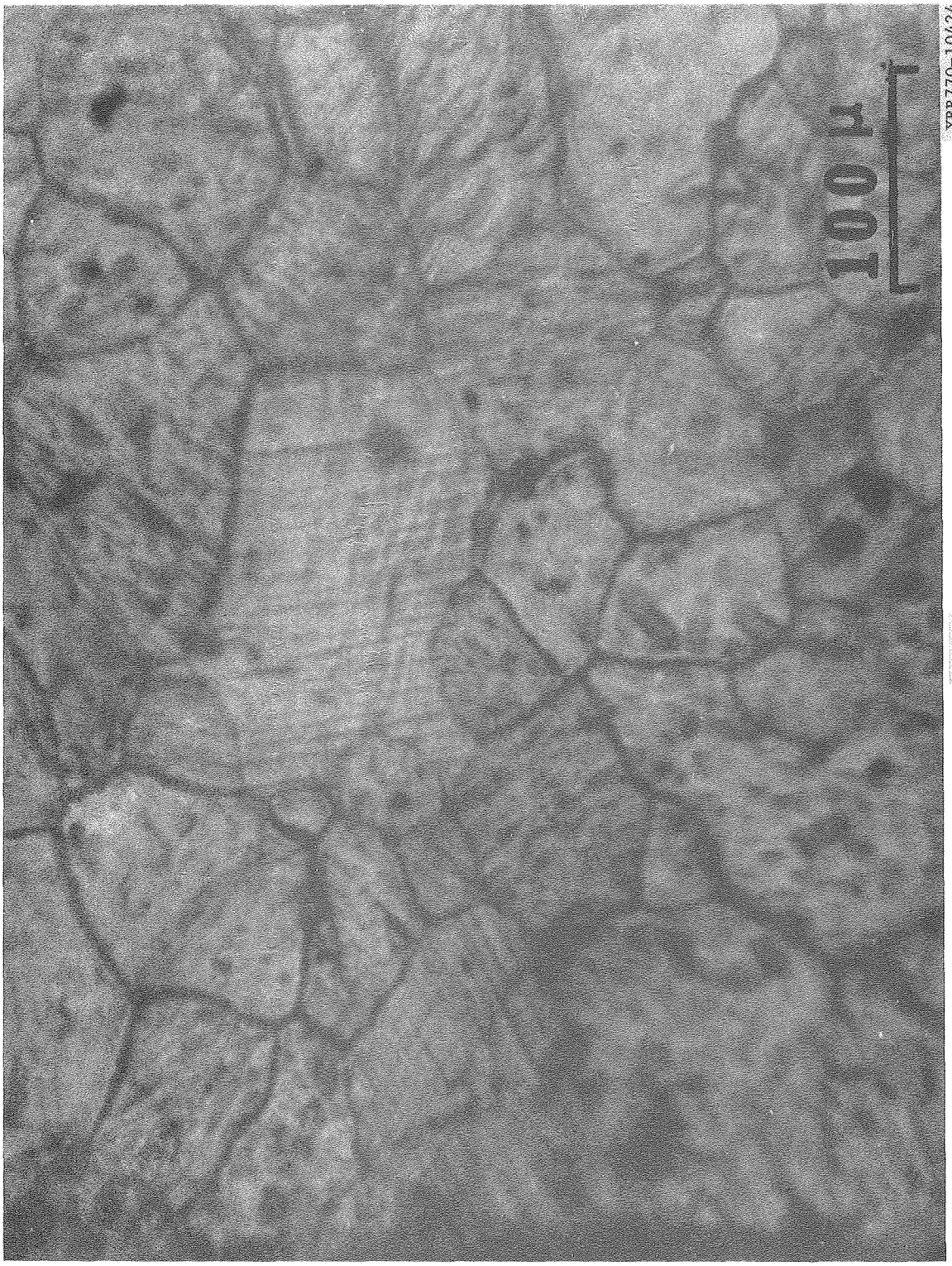

Fig 14

This report was done with support from the United States Energy Research and Development Administration. Any conclusions or opinions expressed in this report represent solely those of the author(s) and not necessarily those of The Regents of the University of California, the Lawrence Berkeley Laboratory or the United States Energy Research and Development Administration.

0 0 0 0 4 5 0 2 2 9 4